Evaluating the Performance of IRI and NeQuick Models in HF Ray Tracing for Real-Time Ionospheric Representation

Yushau Muhammad Sulaiman

KEBBI STATE UNIVERSITY OF SCIENCE AND TECHNOLOGY, ALIERO (KSUSTA), NIGERIA.

October 7, 2025



Outline

- Introduction
 - Introduction
 - Aim and objectives
- 2 Methodology
 - Methodology
 - Ray-tracing algorithm
- Results
 - Program GUI
 - Performance Evaluation
 - Statistical Analysis
- 4 Conclusions
 - Conclusions



Introduction

Space weather refers to the changing conditions in space caused by energy and particles emitted by the sun.

Space weather events often deplete the plasma density of the ionosphere upon which causes depression of the maximum usable frequency (MUF).

Ray-tracing as a geometric optic approximation, can be applied to calculate the propagation path of the high frequency (HF) radio wave (3 - 30 MHz).

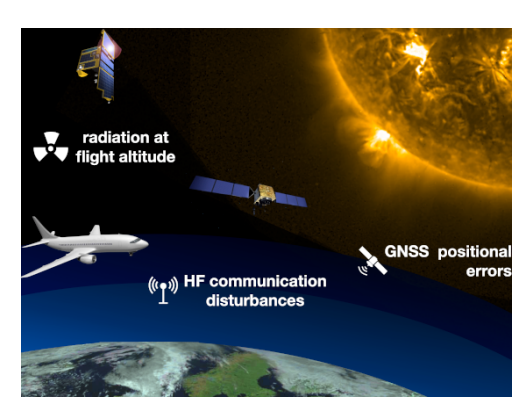


Figure 1. Illustration of modern infrastructures that can be affected by space weather.

Why need for the study?

- For HF communication, accurate simulation of ionospheric conditions through ray-tracing algorithms is essential to predict parameters such as MUF, ensuring reliable and efficient communication.
- This will enable civil aviation and radio broadcasters stay alerts about the possible MUF depression caused by the space weather events.
- A good number of research illustrates the versatility of using ray-tracing in estimating MUF. (e.g Azzarone et al., 2012; Erdem & Feza, 2017; Pietrella et al., 2023).

Aim and objectives

The aim of this research is to evaluate the performance of IRI and NeQuick ionospheric models in HF ray-tracing algorithms. The specific objectives are:

Aim and objectives

The aim of this research is to evaluate the performance of IRI and NeQuick ionospheric models in HF ray-tracing algorithms. The specific objectives are:

- to develop a ray tracing program that, when supplied with ionospheric electron densities, will display the path of a given HF propagation.
- to estimate the range of transmissions and usable frequencies of HF propagation from a given location.
- to compare the range of transmissions predicted using electron density supplied by IRI and NeQuick models.

Data sources

- The IRI2020 model was downloaded from the international reference ionosphere website (https://irimodel.org/).
- The NeQuick version 2.0.2 was obtained from the Aeronomy and Radiopropagation Laboratory of the Abdus Salam International Centre for Theoretical Physics, Trieste, Italy.
- The electron density data was obtained by implementing the IRI and NeQuick executables which is compiled from the FORTRAN source code. This allows for automation of the process required to generate the large amount data used in this work.
- The data processing and visualization were done using MATLAB. (See https://www.mathworks.com/products/matlab.html)

The first step is to quantify the plasma frequency and refractive indices of the ionosphere.

$$\omega_p = \sqrt{\frac{N_e e^2}{m_e \, \varepsilon_0}} \tag{1}$$

$$\mu = \sqrt{1 - \frac{\omega_\rho^2}{\omega^2}} \tag{2}$$

$$\phi_i = \arcsin\left(\sin\phi_1\cos\delta + \cos\phi_1\sin\delta\cos\theta\right) \quad (3)$$

$$\lambda_i = \lambda_1 + \operatorname{atan2} \left(\sin \theta \sin \delta \cos \phi_1, \cos \delta - \sin \phi_1 \sin \phi_i \right)$$
 (4)

$$d = R \times 2\arcsin\left(\sqrt{\sin^2\!\left(\frac{\Delta\phi}{2}\right) + \cos\phi_1\cos\phi_2\sin^2\!\left(\frac{\Delta\lambda}{2}\right)}\right)$$

$$\mu_1 \sin \psi_i = \mu_2 \sin \psi_r \tag{6}$$

$$RMSD_{2D} = \sqrt{\frac{1}{N} \sum_{i=1}^{N} \left[(x_i^{IRI} - x_i^{NQ})^2 + (y_i^{IRI} - y_i^{NQ})^2 \right]}$$

The first step is to quantify the plasma frequency refractive indices the ionosphere.

Next, we used Napier's circle and determine the spherical distance from transmitter to the incident point.

$$\omega_p = \sqrt{\frac{N_e e^2}{m_e \, \varepsilon_0}} \tag{1}$$

$$\mu = \sqrt{1 - \frac{\omega_p^2}{\omega^2}}$$

$$n(\sin \phi_1 \cos \delta + \cos \phi_1 \sin \delta \cos \theta)$$
 (2)

$$\phi_i = \arcsin\left(\sin\phi_1\cos\delta + \cos\phi_1\sin\delta\cos\theta\right)$$

$$\lambda_i = \lambda_1 + \operatorname{atan2} \left(\sin \theta \sin \delta \cos \phi_1, \cos \delta - \sin \phi_1 \sin \phi_i \right)$$
(4)

$$d = R \times 2\arcsin\left(\sqrt{\sin^2\left(\frac{\Delta\phi}{2}\right) + \cos\phi_1\cos\phi_2\sin^2\left(\frac{\Delta\lambda}{2}\right)}\right)$$
(5)

$$\mu_1 \sin \psi_i = \mu_2 \sin \psi_r \tag{6}$$

$$RMSD_{2D} = \sqrt{\frac{1}{N} \sum_{i=1}^{N} \left[(x_i^{IRI} - x_i^{NQ})^2 + (y_i^{IRI} - y_i^{NQ})^2 \right]}$$

The first step is to quantify the plasma frequency refractive indices the ionosphere.

Next, we used Napier's circle and determine the spherical distance from transmitter to the incident point.

We used Harversine equation for the great circle to determine the spherical distance.

$$\omega_{p} = \sqrt{\frac{N_{e}e^{2}}{m_{e}\,\varepsilon_{0}}} \tag{1}$$

$$\mu = \sqrt{1 - \frac{\omega_p^2}{\omega^2}}$$
(2)

$$\mu = \arcsin(\sin\phi_1\cos\delta + \cos\phi_1\sin\delta\cos\theta)$$
(3)

$$\phi_i = \arcsin\left(\sin\phi_1\cos\delta + \cos\phi_1\sin\delta\cos\theta\right)$$

$$\lambda_i = \lambda_1 + \operatorname{atan2} \left(\sin \theta \sin \delta \cos \phi_1, \cos \delta - \sin \phi_1 \sin \phi_i \right)$$
 (4)

$$d = R \times 2\arcsin\left(\sqrt{\sin^2\left(\frac{\Delta\phi}{2}\right) + \cos\phi_1\cos\phi_2\sin^2\left(\frac{\Delta\lambda}{2}\right)}\right)$$
(5)

$$\mu_1 \sin \psi_i = \mu_2 \sin \psi_r \tag{6}$$

$$\mathrm{RMSD}_{2D} = \sqrt{\frac{1}{N}\sum_{i=1}^{N}\left[(x_i^{\mathrm{IRI}} - x_i^{\mathrm{NQ}})^2 + (y_i^{\mathrm{IRI}} - y_i^{\mathrm{NQ}})^2\right]}$$

The first step is to quantify the plasma frequency refractive indices the ionosphere.

Next, we used Napier's circle and determine the spherical distance from transmitter to the incident point.

We used Harversine equation for the great circle to determine the spherical distance.

We applied Snell's law for ionospheric refraction.

$$\omega_{p} = \sqrt{\frac{N_{e}e^{2}}{m_{e}\,\varepsilon_{0}}} \tag{1}$$

$$\mu = \sqrt{1 - \frac{\omega_p^2}{\omega^2}}$$

$$\epsilon = \arcsin(\sin\phi_1\cos\delta + \cos\phi_1\sin\delta\cos\theta)$$
 (2)

$$\phi_i = \arcsin\left(\sin\phi_1\cos\delta + \cos\phi_1\sin\delta\cos\theta\right)$$

$$\lambda_i = \lambda_1 + \operatorname{atan2} \left(\sin \theta \sin \delta \cos \phi_1, \cos \delta - \sin \phi_1 \sin \phi_i \right)$$
(4)

$$d = R \times 2\arcsin\left(\sqrt{\sin^2\left(\frac{\Delta\phi}{2}\right) + \cos\phi_1\cos\phi_2\sin^2\left(\frac{\Delta\lambda}{2}\right)}\right)$$
(5)

$$\mu_1 \sin \psi_i = \mu_2 \sin \psi_r \tag{6}$$

$$RMSD_{2D} = \sqrt{\frac{1}{N} \sum_{i=1}^{N} \left[(x_i^{IRI} - x_i^{NQ})^2 + (y_i^{IRI} - y_i^{NQ})^2 \right]}$$
(7)

- When $\omega_p > \omega$, reflection occurs.No real refraction angle exists the wave is reflected back.
- When $\omega_p < \omega$, refraction occurs. The signal bends away from the normal, and as $\omega \to \omega_p$, the refracted angle approaches 90°.
- When $\omega_p=\omega$, $\psi_r=90^\circ$, signal grazes through the interface of the two media.

- When $\omega_p > \omega$, reflection occurs.No real refraction angle exists the wave is reflected back.
- When $\omega_p < \omega$, refraction occurs. The signal bends away from the normal, and as $\omega \to \omega_p$, the refracted angle approaches 90°.
- When $\omega_p = \omega$, $\psi_r = 90^\circ$, signal grazes through the interface of the two media.

Note:

For each ionospheric layer, the maximum frequency that will be reflected back is proportional to the density of its peak layer.

Each layer is assumed to have constant electron density and hence constant refractive index.

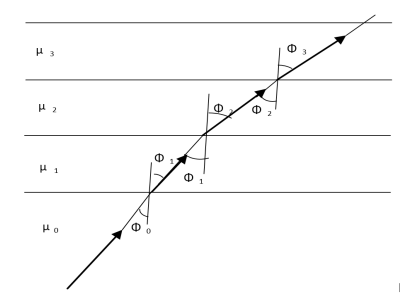


Figure 2. Ionospheric refraction



Each layer is assumed to have constant electron density and hence constant refractive index.

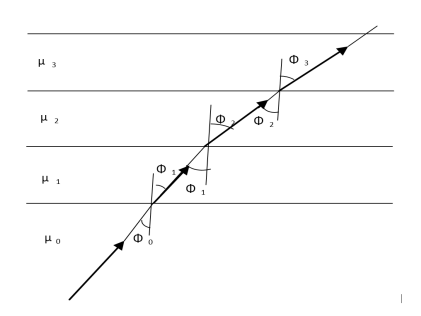


Figure 2. Ionospheric refraction

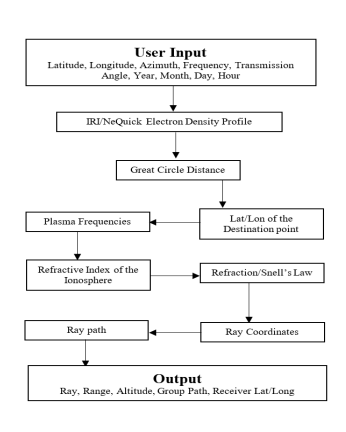


Figure 3. Program work flow

Graphical User Interface (GUI)

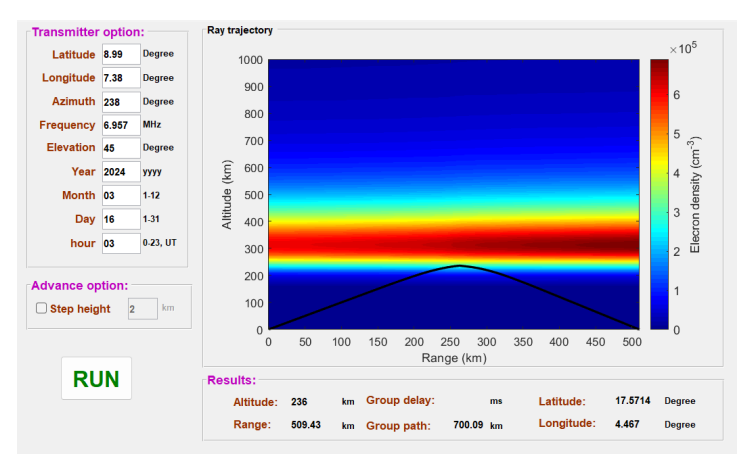


Figure 4. Appearance of the GUI After running the program

Maximum Usable Frequency (MUF)

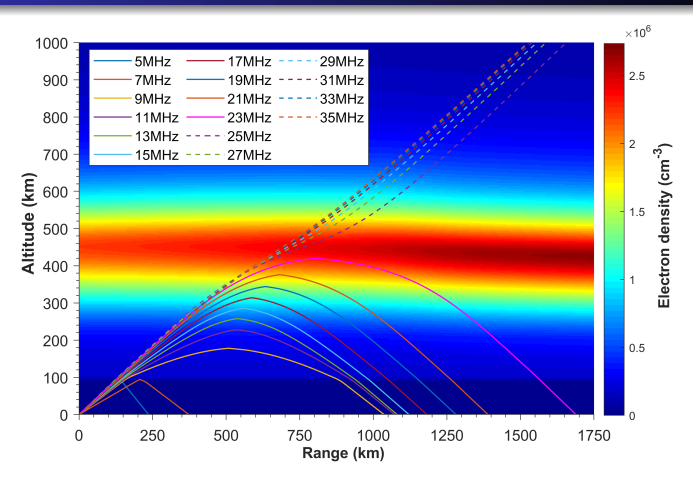


Figure 5. Estimation of MUF from Abuja $(8.99^{\circ}N, 7.38^{\circ}E)$ to Lagos $(6.52^{\circ}N, 3.38^{\circ}E)$. HF of 5 MHz – 35 MHz, at elevation 30° on 30/09/2024, 01:00 UT (Azimuth: 238°).

IRI versus NeQuick

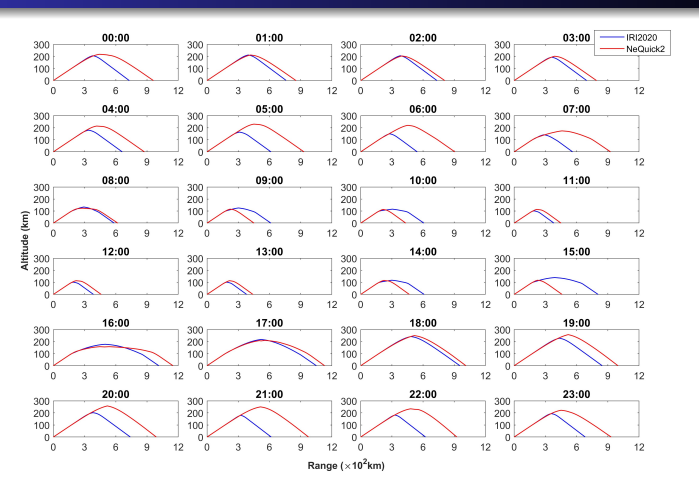


Figure 6. Diurnal prediction of HF transmission range using IRI and NeQuick models. The simulation is done for HF of 6.957 MHz, at elevation 30° on 30/09/2024.

IRI versus NeQuick

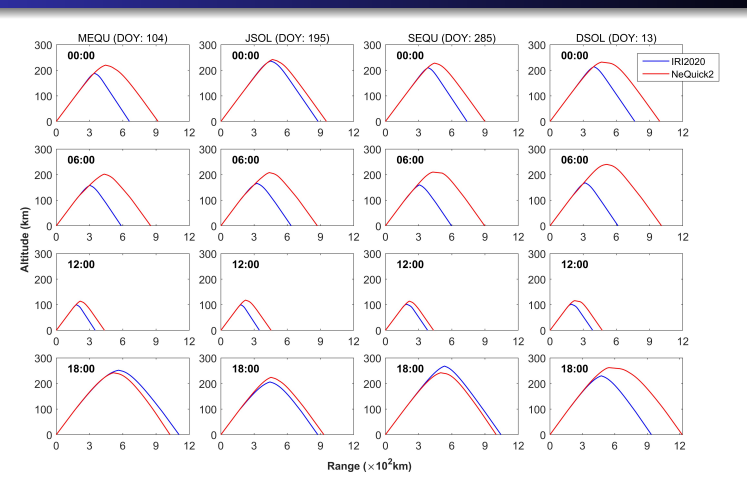


Figure 7. Comparison of HF transmission range over season of the year 2024. The simulation is done for HF of $6.957\,\mathrm{MHz}$, at elevation 30° .

IRI versus NeQuick

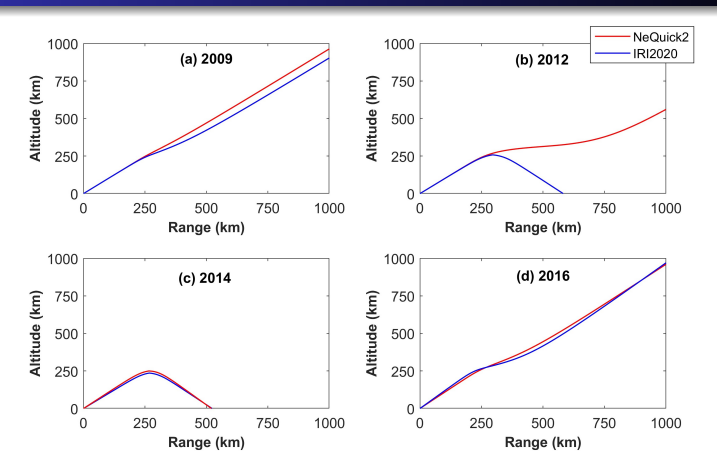


Figure 8. Illustration of HF transmission range as a function of solar activity: (a) low, (b) ascending, (c) high, and (d) descending solar activities. The simulation is done at 18:00 LT for HF of 6.957 MHz, at elevation 30°.

Statistical Analysis

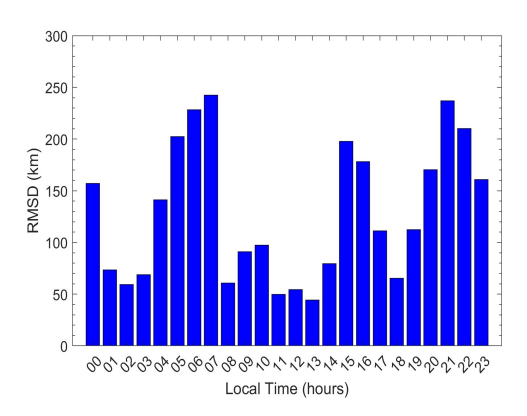


Figure 9. RMSD for model prediction of ray-path

Statistical Analysis

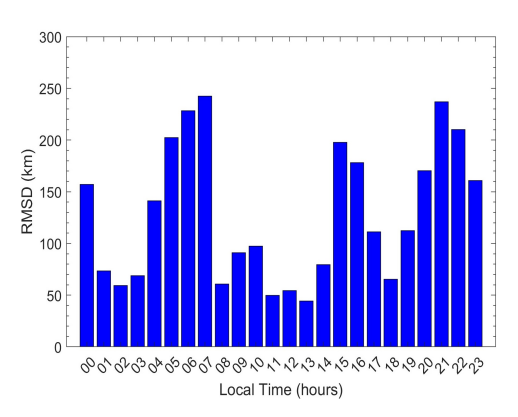


Figure 9. RMSD for model prediction of ray-path

Figure 9 indicates that ray paths are most comparable around midday, 02:00, and 18:00, while the largest differences occur at 07:00 and 21:00. It is consistent with results shown during high solar activity.

Conclusions

- This work presents a simple ray tracing algorithm for the prediction of MUF and range of HF transmission using IRI and NeQuick2 climatological models.
- HF signal of 6.957 MHz, transmitted with elevation greater than 25° are lost to outer space while those with lower elevation reaches the earth at increasingly greater distance.
- Prediction of ray paths using the two models are most comparable around midday, 02:00, and 18:00, while the largest differences occur at 07:00 and 21:00.
- The established climatological models can be integrated into real-time ray tracing tools for improved forecasting and mitigation of ionospheric effects in data sparse areas.

Thank You!